Title

Controls on soil organic matter stability and composition of neutral-to-alkaline topsoil and subsoil across Indo-Gangetic plains

Journal

Catena, 258

ISSN

0341-8162

Authors

Zhong, Ruohan

Lyu, Han

Kumari, Monika

et al.

Publication Date

2025-10-01

DOI

10.1016/j.catena.2025.109215

Peer reviewed

Catena 258 (2025) 109215

Contents lists available at ScienceDirect

Catena

journal homepage: www.elsevier.com/locate/catena

Controls on soil organic matter stability and composition of neutral-to-alkaline topsoil and subsoil across Indo-Gangetic plains

Ruohan Zhong [a], Han Lyu [b,c,*], Monika Kumari [c], Ajay Kumar Mishra [c], M.L. Jat [d,e], Randy A. Dahlgren [f], Shinya Funakawa [a,c], Tetsuhiro Watanabe [a,*]

[a] Graduate School of Agriculture, Kyoto University, Kyoto 606-8502, Japan
[b] Institute of Agriculture, Tokyo University of Agriculture and Technology, Fuchu, Tokyo 183-8509, Japan
[c] Graduate School of Global Environmental Sciences, Kyoto University, Kyoto 606-8501, Japan
[d] International Crops Research Institute for the Semi-Arid Tropics, Patancheru 502324 Telangana, India
[e] International Maize and Wheat Improvement Center, India Office, National Agricultural Science Centre Complex, New Delhi 110012, India
[f] Department of Land, Air and Water Resources, University of California Davis, Davis 95616 CA, USA

ARTICLE INFO

Keywords:
SOC pools
SOM fractions
SOM molecular composition
Active Al/Fe
Topsoil and subsoil
Forest and agriculture

ABSTRACT

Elusive controls over soil organic carbon (SOC) in neutral-to-alkaline soils limit long-term carbon dynamic predictions across vast agricultural areas such as Indo-Gangetic Plain (IGP). We studied the causes of low SOC content in neutral-to-alkaline topsoil and subsoil under tropical to subtropical climates by identifying factors controlling soil organic matter (SOM) fractions, SOC pools, and SOM molecular composition. We investigated topsoil and subsoil from six paired forest and agricultural fields within 12 sites across IGP, using SOM fractionation, 196-day soil incubation, and pyrolysis-GC/MS. A three-pool kinetic model estimated labile, intermediate, and stable SOC pools from respiration curves, with non-hydrolyzable SOC as the stable pool. Measured soil properties include pH, exchangeable cations, CEC, inorganic/organic C, texture, oxalate-extractable Al/Fe (active Al/Fe), and dithionite-extractable Al/Fe. SOC turnover over decades is regulated by the intermediate SOC pool, which is closely associated with mineral-associated SOM. Active Al/Fe, rather than exchangeable Ca^{2+}, clay, or agricultural activity, controlled the stability of intermediate pool in both topsoil and subsoil. In topsoil, agricultural activity reduced light fraction carbon by 38 % and intermediate pool size by 34 %, but had no significant effect in subsoil or on more stable fractions/pools. Active Al/Fe had a stronger effect on stabilizing carbon in less carbon-saturated subsoil. SOM degradation was intense (e.g., high abundance of N-containing compounds) and was attributed to low active Al/Fe levels under drier conditions, and to elevated microbial activity driven by neutral-to-alkaline soil pH. Cultivation had a non-significant influence on SOM composition. In conclusion, the low SOC in neutral-to-alkaline IGP soils is primarily due to drying and elevated pH, which limits active Al/Fe formation, thereby reducing SOC stability and intensifying SOM degradation. Cultivation further exacerbates SOC loss in topsoil. This highlights the need for understanding and targeted management of these SOM regulating factors to enhance ecological and agricultural sustainability in neutral-to-alkaline soils.

1. Introduction

Soil organic matter (SOM) is a primary organic carbon reservoir of terrestrial ecosystems (Lützow et al., 2006). Changes in stocks and mean residence times of SOM could significantly alter terrestrial carbon dynamics, impacting climate change (Schmidt et al., 2011). Beyond its role in global carbon dynamics, SOM is integral to soil health, fertility, and resilience, thereby having a strong influence on ecosystem biodiversity and agricultural productivity (Jia et al., 2023; Tiessen et al., 1994). Notably, significant portions of neutral-to-alkaline soils in tropical and subtropical regions exhibit low soil organic carbon (SOC) content (Lal, 2004; Xu et al., 2021), restricting their ability to support natural forests and sustainable agricultural production (Tiessen et al., 1994). Land-use modifications, particularly shifts from native to agricultural systems, can substantially reduce the SOC pool, often exceeding 60 % or more (Lal, 2010). Consequently, understanding mechanisms for C stabilization in neutral-to-alkaline soils in tropical and subtropical regions is crucial for developing strategies to address climate change and maintain

* Corresponding authors at: Institute of Agriculture, Tokyo University of Agriculture and Technology, Fuchu, Tokyo 183-8509, Japan (H. Lyu).
E-mail addresses: lyuhan1993@gmail.com (H. Lyu), watanabe.tetsuhiro.2m@kyoto-u.ac.jp (T. Watanabe).

https://doi.org/10.1016/j.catena.2025.109215
Received 6 March 2025; Received in revised form 13 May 2025; Accepted 2 June 2025
Available online 8 June 2025

sustainable land use while considering climate, soil properties, and land-use practices.

The interplay of climate-driven microbial decomposition and climate-influenced mineral stabilization controls SOM dynamics. Warm, moist conditions speed microbial breakdown of organic matter (Zhang et al., 2020), yet the same high rainfall/moisture can lead to increased base-cation leaching, reduced soil pH, and promote the formation of active Al/Fe (oxalate-extractable Al/Fe) that stabilizes SOM (Lyu et al., 2018; Lyu et al., 2022). The active Al/Fe phases, encompassing short-range-ordered Al/Fe minerals, active sites of Al/Fe hydroxides, and organo-Al/Fe complexes, are potent sorbents that protect SOM in many acidic and volcanic soils (Rasmussen et al., 2018). Under drier climates or in landscapes receiving carbonate, pH rises, base cations (e.g., Ca^{2+}, Mg^{2+}) accumulate, and SOM stabilization may be regulated by cation-bridging of organic matter to clay surfaces (Neina, 2019). Fine soil mineral fractions (i.e., silt and clay) provide additional stability to organic matter through organo-mineral interactions and aggregation (Rodrigues et al., 2022b). Although active Al/Fe is a proven SOM stabilizer in acidic soils, its relative importance in neutral to alkaline soils with drier climates, where clay surfaces and Ca/Mg bridging may prevail, remains uncertain.

SOM is not a uniform entity but a complex mixture of different components that vary in turnover rates and chemical properties (Trumbore, 2000). By partitioning SOC into pools with different stabilities, researchers can identify controls on the labile pool, which is susceptible to rapid microbial decomposition, and the stable pool, which is largely protected from decomposition due to various physical, chemical, and biological mechanisms (Six and Jastrow, 2002). This partitioning is vital for understanding the factors controlling SOC content and stability, as well as the resilience of soils to external perturbations, such as land-use change or climatic variations (Doetterl et al., 2015).

Distinct differences exist between topsoil and subsoil horizons regarding their SOC pools and C-saturation status are crucial for understanding SOC stabilization mechanisms and potential SOC sequestration capacity (Possinger et al., 2021; Rodrigues et al., 2022b). Subsoil horizons typically have a lower C-saturation status and SOC stabilization depends more on interactions with soil minerals (Yu et al., 2017). However, studies examining topsoil versus subsoil differences on SOC dynamics in neutral-to-alkaline soils in tropical and subtropical regions remain particularly scarce. Also, changes in land-use, especially from natural vegetation to agricultural land, can significantly impact SOC dynamics (John et al., 2005; Lozano-García et al., 2017). Hence, the convergence of climatic and soil factors with human-induced ecosystem alterations poses several pertinent questions about SOC content and ecosystem/agricultural sustainability.

Understanding SOM molecular composition is key to SOC dynamics. Specific organic molecules in SOM are linked to climatic and soil factors and vary in decomposition rates, reflecting complex SOC stabilization and mineralization mechanisms (Angst et al., 2021; Lehmann and Kleber, 2015). For instance, aromatic monomers are indicators of increased SOM stability (Dungait et al., 2012), whereas saccharides and fatty acids, though susceptible to degradation, persist in soils due to stabilization by clay minerals (Buurman and Roscoe, 2011; Keiluweit et al., 2015). Modern SOC models face uncertainties due to limited knowledge of SOM composition and sequestration mechanisms (Davidson and Janssens, 2006; Kleber et al., 2021). Therefore, it is imperative to focus on factors affecting SOM molecular composition, which can be investigated at high resolution using analytical pyrolysis, as they directly influence SOC content and stability.

The varied climate (from semi-arid to humid monsoon) and soil textural gradients (coarser upstream and finer downstream) in the Indo-Gangetic Plain (IGP), make it an ideal region to study SOC stabilization mechanisms of neutral-to-alkaline soils (Pal et al., 2009). The region features intensive agriculture alongside patches of natural vegetation, creating a mosaic of land-use types (Pal et al., 2009; Wikramanayake, 2002) that may influence SOC content. More than 90 % of the IGP area is agricultural land and produces more than 40 % of rice and 70 % of wheat for India (Shah et al., 2019; Singh et al., 2023). The low SOC content (4.2 ± 0.9 g kg^{-1}: mean ± SD) in IGP soils, which constrains agricultural productivity (Lal, 2004), further emphasizes the relevance of this study toward promoting sustainable agricultural practices. By investigating the climatic and soil properties, especially active Al/Fe and fine mineral particles, that regulate SOC content with the consideration of land use changes, this research will contribute to promoting sustainable agricultural practices in neutral-to-alkaline soils across tropical and subtropical regions.

This study aimed to elucidate the factors contributing to low SOC levels in the neutral-to-alkaline soils by analyzing topsoil and subsoil along a climate-elevational gradient in the IGP. We focus on understanding how climate, changes in soil properties along river flow, and shifts from natural vegetation to agricultural land affect the size and stability of SOC pools, as well as the SOM molecular composition. We hypothesized high pH and low active Al/Fe content are primary determinants of low SOC levels in neutral-to-alkaline topsoil and subsoil, like IGP soils. These conditions limit the size and stability of intermediate and stable SOC pools by reducing organo-mineral associations and promoting SOM degradation. Secondly, we hypothesized that subsoil SOM, while more degraded, is more strongly stabilized through specific mineral associations, particularly with active Al/Fe phases, compared to topsoil. We further conjectured that agricultural activity disproportionately reduces the intermediate SOC pool and alters SOM molecular composition in topsoil, where active Al/Fe-mediated stabilization is limited under neutral-to-alkaline conditions.

2. Materials and Methods

2.1. Study sites and soils

Study sites, identical to those in our previous study (Zhong et al., 2023), spanned three distinct agro-climatic zones in the IGP of India, namely the upper, middle, and lower IGP, totaling 12 sites (22°17′44.3″–29°16′23.8″N, 77°45′27.3″–89°33′12.3″E). The 12 sites were selected from 23 sites that had been determined, in consultation with local soil scientists, to represent soils in each region. Sampling was conducted from mid-November to early December, corresponding to the dry season and post-harvest slack season, when light fraction spikes from residue incorporation may attenuate. Within each zone, two representative sites were selected due to the limited availability of uncultivated land and to minimize redundancy by excluding sites with similar soil properties (unpublished survey data). Although site numbers per zone are limited, key soil properties vary little across the IGP. The selected sites capture major pedoclimatic gradients relevant to SOC stabilization. While not fully representing all non-acidic soils, this framework allows robust analysis of SOC mechanisms. Sampling sites, labeled I1 to I6 from the upper to lower IGP (Fig. S1), span an elevation and depositional gradient from 224 m to 5 m asl, with mean annual temperature and precipitation ranging from 24.1–26.5 °C and 840–3290 mm, respectively, thus capturing a representative moisture gradient (Table 1).

Soil samples were obtained from typical agricultural land and secondary forest (non-managed forest/shrub vegetation, Table 1) for each site by making soil profiles. The forest sites (including shrub vegetation) had at least 20 years of continuous tree/shrub cover without cultivation. Moving from west-to-east, elevation declines while annual precipitation rises. Soils have a hyperthermic temperature regime and ustic moisture regime, developed from mixed alluvial deposits, and are identified as Gleysols, Cambisols, or Luvisols (IUSS Working Group WRB, 2022) (Table 1). Clay mineralogy consistently featured mica, vermiculite, kaolinite, and smectite, with specific sites like I3 having more smectite and I5 displaying higher kaolinite levels.

Soils were sampled from profiles reaching roughly 1 m deep. Though

Table 1
Site characterization information for soil sampling locations in Indo-Gangetic Plain (IGP).

Region of IGP	Location	Coordinates	Elevation	MAT[a]	MAP	Soil type	Forest type	Cropping pattern in cropland
			m	°C	mm			
Upper	Meerut (I1)	F[a]: 29°16′16.8″N, 77°45′59.4″E A: 29°16′23.8″N, 77°45′27.3″E	224	24.1	970	Luvisols	Secondary forest to bush	Wheat, sugarcane, vegetables
	Kanpur (I2)	F: 26°23′53.7″N, 79°53′5.8″E A: 26°23′54.1″N,79°53′10.6″E	126	25.7	840	Luvisols	Secondary forest to bush	Wheat, sugarcane, vegetables
Middle	Patna (I3)	F: 25°35′26.8″N, 84°45′7.8″E A: 25°35′47.7″N, 84°45′7.4″E	55	25.7	1050	Cambisols	Secondary forest to bush	Rice, wheat, maize, barley, millet
	Samastipur (I4)	F: 25°49′3.9″N, 85°40′8.3″E A: 25°49′3.2″N, 85°40′8.6″E	53	24.9	1000	Cambisols	Secondary forest to bush	Rice, wheat, maize, barley, millet
Lower	Coochbehar (I5)	F: 26°32′56.6″N,89°33′2.4″E A: 26°32′54.6″N,89°33′12.3″E	42	24.9	3290	Cambisols	Secondary forest	Rice, vegetables
	Canning town (I6)	F: 22°18′5.2″N,88°39′59.7″E A: 22°17′44.3″N,88°45′1.3″E	5	26.5	1700	Gleysols	Secondary forest	Rice, vegetables

Soil type classification based on the World Reference Base for Soil Resources (IUSS Working Group WRB, 2022).
[a] F, forest field; A, agricultural field; MAT, mean annual temperature; MAP, mean annual precipitation.

samples from all horizons were collected, this study focused on both topsoil and subsoil horizons (0–15 cm and 40–60 cm, respectively) due to their distinct differences in SOC pools and C-saturation status. Also, the 0–15 cm horizon represents the cultivated layer (tillage ≤ 20 cm) receiving fresh C inputs, whereas the 40–60 cm is an undisturbed subsoil horizon. The intermediate (15–40 cm) horizon showed soil properties (e.g., pH, texture, active Al/Fe, and C-saturation status) intermediate between top- and subsoils (40–60 cm) (unpublished profile data); thus, focusing on these end-members maximized the topsoil–subsoil contrast while keeping the study practical. A total of 24 soil samples were collected and categorized into four groups: forest topsoil (FT), forest subsoil (FS), agricultural topsoil (AT), and agricultural subsoil (AS). Air-dried soils were sieved through a 2-mm mesh and thoroughly mixed for further analysis.

2.2. Climate

The climate information of the study sites was provided in Table 1. Temperature and precipitation were obtained from WorldClim (Fick and Hijmans, 2017). We calculated annual excess precipitation (EP) by subtracting potential evapotranspiration from monthly precipitation (Lyu et al., 2018). For each sampling point, potential evapotranspiration was calculated using solar radiation and monthly air temperature (Harkin, 1960; Thornthwaite, 1948).

2.3. Soil physicochemical properties

Measured soil physicochemical properties included pH, exchangeable cations (Ca^{2+}, Mg^{2+}, K^{+}, and Na^{+}), cation exchange capacity, total C and N, inorganic carbon (IC), SOC, dissolved organic carbon (DOC), soil particle-size distribution (sand, silt, and clay contents). Active Al/Fe (Al_o and Fe_o) were extracted by acid oxalate. Free Fe hydroxides (Fe_d) were determined by extraction with combined citrate and sodium dithionite. Crystalline Fe (hydro)oxides were calculated by subtracting Fe_o from Fe_d. Details for soil physicochemical properties measurements are in Supplementary Materials 1.1.

2.4. Soil organic matter fractionation

SOM fractionation utilized the following procedures (Lyu et al., 2021a; Zhong et al., 2023): Density separation (1.6 g cm^{-3}) partitioned SOM into light (LF) and heavy (HF) fractions. After sodium hexametaphosphate dispersion and a 15-hour shake, the HF was further separated by particle size into mineral-associated organic matter (MAOM, <53 μm) and occluded particulate organic matter (oPOM, ≥53 μm). MAOM fraction underwent a 6 M HCl reflux at 115 °C for 16 h to identify the non-hydrolyzable SOM in the MAOM fraction. Weight and C content of each fraction were subsequently measured.

2.5. Soil incubation and SOC pool partitioning

We conducted incubation experiments on both topsoil and subsoil to obtain a carbon mineralization curve for SOC. Three replications of 20 g soil (dry weight basis) were placed in sealed 225 mL glass mason jars and maintained moisture to 55 % of water holding capacity (WHC). WHC was measured by fully saturating the soil, placing it on filter paper in a glass funnel, and allowing it to drain for 12 h. The gravimetric moisture content of the drained sample, taken as 100 % WHC, was then determined after oven-drying at 105 °C for 24 h. The CO_2 collection commenced following a 7-day pre-incubation at 25 °C (Lyu et al., 2021a).

The CO_2 released from soils was captured using 10 mL of 1 M NaOH solution inside a plastic bottle within the incubation jar. Over the 196-day incubation period, the CO_2 captured by the NaOH was collected, and CO_2 emissions were determined through titration with 0.05 M HCl. The alkaline solution was sampled on days 7, 14, 28, 49, 70, 91, 112, 140, 168, and 196 to determine cumulative CO_2 release curves.

By fitting cumulative CO_2 release curves to a first-order kinetic model, SOC pool partitioning was done as follows (Lyu et al., 2021a):

$$C_r = 1 - C_L\% \times e^{-\left(\frac{1}{MRT_L}\right)\times t} - C_I\% \times e^{-\left(\frac{1}{MRT_I}\right)\times t} - C_S\% \times e^{-\left(\frac{1}{MRT_S}\right)\times t} \quad (1)$$

In this equation, C_r represents the ratio of cumulative CO_2 release to total SOC of day t. C_L%, C_I%, and C_S% denote the labile pool, intermediate pool, and stable pool proportions. MRT_L, MRT_I, and MRT_S (days) represent the mean residence time (MRT) for each pool. The C_S% value was derived from the proportion of non-hydrolyzable MAOM C to SOC. Relying on prior research and enhanced fitting accuracy (Lyu et al., 2021a; Wiedemeier et al., 2012), we set a value of 1000 years for the MRT_S constant in Eq. (1).

The Universal Global Optimization Algorithm (Auto2Fit 5.5, 7D-Soft High Technology, China) was employed for nonlinear regression of Eq. (1) with specific constraints: MRT_L = [1, 100] and MRT_I = [1000, 100000] (days), which are the same constraints used in our previous studies (Lyu et al. 2021a, b). The sizes of labile (C_L), intermediate (C_I), and stable (C_S) SOC pools were calculated as proportions relative to the total SOC.

Values of SOC pools for soils from tropical volcanic regions reported in our previous study (Lyu et al. 2021b)—characterized by high active Al/Fe and a large stable SOC pool with acid soil pH—were compiled only as qualitative benchmarks. These reference data were served in the discussion (1) to illustrate how reactive Al/Fe can control SOC pools and (2) to contrast with the low–Al/Fe, low stable SOC pool status of IGP

neutral-to-alkaline soils.

2.6. One-shot Py-GC/MS

Molecular composition of soil organic compounds was examined using pyrolysis–gas chromatography–mass spectrometry (Py-GC/MS) (Lyu et al., 2024). Air-dried bulk soils were finely ground and homogenized using a ball mill (PM100, Retsch, Germany). Pyrolysis analysis was conducted using GC/MS (GCMS-QP2020, Shimadzu, Japan) combined multi-functional pyrolyzer (EGA/PY3030D, Frontier Lab, Japan). Soils containing approximately 100 μg C were subjected to pyrolysis (550 °C; one minute). Post-pyrolysis, volatile compounds were cryo-trapped at −180 °C using a MicroJet Cryo-Trap (MJT-1035E, Frontier Lab), followed by rapid thermal desorption for subsequent analysis. Pyrolysis products were processed using a capillary column (Ultra ALLOY^{+}-5, Frontier Lab). The GC oven temperature was initially set at 50 °C for 1 min, then increased to 300 °C at a rate of 10 °C per minute, and held at 300 °C for 5 min. Helium served as the carrier gas, flowing through the column at 1 mL per minute. Mass spectra were scanned across the 29–800 *m/z* mass range with electron ionization. The top 100 peaks were integrated, and those contributing more than 80 % of the total area were identified using the NIST 17 library and personal reference list (Table S1).

Identified compounds were divided into 16 groups (Table S1): undegraded polysaccharides (PS), degraded PS, long alkanes, short alkanes, n-alkenes, squalene, fatty acids and esters (FAnE), steroids, lignin, phenols, monocyclic aromatic hydrocarbons (MAH), polycyclic aromatic hydrocarbons (PAH), alkylamides, N-containing MAH (N-MAH), other N-containing compounds (N-containing), and other hydrocarbons. The relative abundance of each group was determined by calculating the ratio of its chromatogram peak area (within the *m/z* range of 29–550) to the total area of identified compounds.

2.7. Statistical analyses

Given that many parameters remained non-normally distributed even after log transformation, we employed Spearman rank correlation analysis, which does not require the assumption of normality and is robust to outliers. We included land use and horizon, coding them as binary variables (forest soil: 1, agricultural soil: 0; topsoil: 1, subsoil: 0), in the Spearman rank correlation analysis. Differences in overall soil properties and SOM compositions between forest and agricultural sites or between topsoil and subsoil were assessed using Bray-Curtis distance-based PERMANOVA with nonmetric multidimensional scaling (NMDS). A pairwise *t*-test was applied to assess differences in soil properties, SOM fractions, SOC pools, and SOM compound groups by land use and soil horizon. Kruskal-Wallis test was applied to evaluate the overall differences among the groups, followed by Dunn's post-hoc tests without Bonferroni correction. To assess the influence (both direction and magnitude) of land use and climatic and soil properties on SOC pools while excluding confounding factors, we employed partial least squares path modeling (PLS-PM) using the "SEMinR" package (Hair et al., 2021). PLS-PM was conducted based on correlations and potential influencing mechanisms. The significance of path coefficients in the final PLS-PM was ascertained through the bootstrapping method (nboot = 999). Redundancy analysis (tb-RDA) was applied to clarify relationships between SOM compound groups and climatic and soil properties with 999 permutations. For both PLS-PM and tb-RDA, we employed variance inflation factor (VIF) tests and stepwise selection to determine the optimal influencing factors, considering single correlations. NMDS, PERMANOVA, and tb-RDA were conducted with "vegan" and "microeco" packages (Liu et al., 2021; Oksanen et al., 2020). All statistics utilized R version 4.3.1. Significance levels were denoted as *, **, and *** for *P* values < 0.05, <0.01, and < 0.001, respectively. Values are reported as the mean ± SD, unless otherwise noted.

3. Results

3.1. Climatic and soil physicochemical properties

Table S2 summarizes the climatic and soil properties of each sampling location. As proximity to the Indian Ocean increases with a corresponding decrease in elevation, mean annual precipitation (MAP) and EP increase (r_s = −0.83*** and −0.60**, Fig. S2). Forest and agricultural soils showed minimal differences in physicochemical properties as demonstrated by PERMANOVA analysis (Fig. S3). Topsoil and subsoil pH ranged from 6.2 to 9.9 and 5.7 to 9.2, respectively, with a decreasing trend from upper to lower IGP, corresponding with increasing precipitation and base-cation leaching (Fig. S2). Inorganic C contents were high for both topsoil and subsoil of I4 (Table S2), where remnant carbonate shells were found. While exchangeable Na^{+} (0.29 ± 0.25 $cmol_c\ kg^{-1}$) and K^{+} (0.21 ± 0.21 $cmol_c\ kg^{-1}$) were low, exchangeable Ca^{2+} (11.7 ± 10.4 $cmol_c\ kg^{-1}$) and Mg^{2+} (3.3 ± 3.0 $cmol_c\ kg^{-1}$) were much higher, indicating a low risk of adverse effects from sodic soil conditions (i.e., low exchangeable Na^{+} percentages).

Across all sites, oxalate-extractable Al and Fe content (active Al/Fe) was consistently low, measuring less than 14 cmol kg^{-1}. Notably, the molar ratio of SOC to (Al_o + Fe_o) was significantly higher ($P < 0.01$) in topsoil (25.5 ± 18.8) than that in subsoil (7.3 ± 3.3). Although topsoil displayed similar levels of active Al/Fe, exchangeable Ca^{2+}/Mg^{2+}, and clay contents as the subsoil, Fe_d − Fe_o was lower in topsoil (Table 2). Active Al/Fe content was higher in lower IGP, correlating positively with MAP and EP and negatively with soil pH (Fig. S2). When analyzed separately, both topsoil and subsoil displayed similar relationships of active Al/Fe with MAP and pH (Fig. S4). Moreover, clay + silt and clay contents increased along the river flow, with soil textures primarily being silty loam in the upper IGP and transitioning to silty clay loam and clay in the lower IGP (Fig. S5).

Comparing the two horizons, topsoil showed a significantly higher SOC (13.5 ± 6.6 g kg^{-1}) relative to subsoil (3.7 ± 0.9 g kg^{-1}) across all sites (Table 2). In subsoil, SOC showed positive relationships with Mg_{ex},

Table 2
Comparison of soil properties (mean ± SD, n = 12) between topsoil and subsoil.

	Unit	Topsoil	Subsoil	*P* value of paired *t*-test
pH		7.7 ± 1.1	8.0 ± 1.1	0.258
CEC	$cmol_c\ kg^{-1}$	10.1 ± 4.5	10.2 ± 5.0	0.936
SOC	g kg^{-1}	13.5 ± 6.6	3.7 ± 0.9	<0.001
IC	g kg^{-1}	3.9 ± 6.6	0.3 ± 1.1	0.060
TN	g kg^{-1}	1.1 ± 0.6	0.3 ± 0.2	0.001
C:N ratio		13.0 ± 4.2	15.1 ± 4.4	0.261
DOC	g kg^{-1}	0.19 ± 0.09	0.06 ± 0.02	<0.001
Ca_{ex} + Mg_{ex}	$cmol_c\ kg^{-1}$	15.6 ± 11.6	14.3 ± 10.4	0.526
Ca_{ex}	$cmol_c\ kg^{-1}$	12.4 ± 11.4	10.9 ± 9.7	0.473
Mg_{ex}	$cmol_c\ kg^{-1}$	3.2 ± 3.3	3.4 ± 2.9	0.530
Clay + Silt	%	81 ± 15	82 ± 16	0.555
Clay	%	23 ± 13	23 ± 7	0.918
Al_o + Fe_o	cmol kg^{-1}	6.2 ± 4.0	5.1 ± 2.6	0.141
Fe_o	cmol kg^{-1}	3.9 ± 2.9	3.0 ± 2.0	0.086
Al_o	cmol kg^{-1}	2.2 ± 1.3	2.1 ± 0.7	0.508
SOC/(Al_o + Fe_o)	mol mol^{-1}	25.5 ± 18.8	7.3 ± 3.3	0.002
Fe_d	cmol kg^{-1}	14.3 ± 6.0	18.5 ± 9.2	0.023
Fe_d − Fe_o	cmol kg^{-1}	10.4 ± 4.1	15.4 ± 7.8	0.002

CEC, cation exchange capacity; SOC, soil organic carbon; IC, inorganic carbon; TN, total nitrogen; C:N ratio, ratio of SOC to TN; DOC, dissolved organic carbon; Ca_{ex} and Mg_{ex}, exchangeable Ca^{2+} and Mg^{2+}; Al_o + Fe_o, acid oxalate extractable active Al and Fe; Fe_d, dithionite-citrate extractable iron; Fe_d − Fe_o, crystalline Fe (hydr)oxides.

clay + silt, clay, and Fe_o ($r_s = 0.80^{**}$, 0.61^{*}, 0.66^{*}, 0.67^{*}, respectively), and a near-significant association with active Al/Fe ($r_s = 0.53$, $P = 0.08$). Notably, topsoil SOC content was only significantly correlated with TN, IC, and DOC (Fig. S4a). Across all soils, no significant correlation emerged between SOC and variables such as land use, elevation, and climate (Figs. S2 and S4).

3.2. SOM fractionation and SOC pools

Fig. 1 presents the SOC content and proportion of each SOM fraction. Overall, organic carbon factors (i.e., SOC, DOC, SOM fractions, and SOC pools) were similar between agricultural and forest soils, as indicated by NMDS diagrams and confirmed by the PERMANOVA test (Fig. S6). For SOM fractions, only the LF carbon content, a minor part of total SOC, was higher in forest soils than in agricultural soils (Fig. 1ab). The MAOM (9.5 ± 6.1 g C kg^{-1}), LF (1.8 ± 1.1 g C kg^{-1}), and oPOM (0.6 ± 0.4 g C kg^{-1}) contents were significantly higher in topsoil than subsoil (2.6 ± 0.9, 0.3 ± 0.3, $0.1 \pm <0.1$ g C kg^{-1}, respectively), with MAOM representing the majority (68 ± 15 %) among all fractions. Non-hydrolyzable MAOM content was similar for topsoil and subsoil, yet it constituted a larger proportion in subsoil (Fig. 1cd).

Curves of cumulative CO_2 release across all sites are shown in Fig. S7. Respiration rates were higher in the first two months for topsoil and the first month for subsoil, after which CO_2 released steadily. Cumulative CO_2 release curves (Fig. S7) fit Eq. (1) effectively, with RMSE < 0.001, SSR $< 10^{-5}$, and r and R^2 values exceeding 0.995.

Table 3 presents the size, proportion, and mean residence time (MRT) of each SOC pool. The size of intermediate SOC pool was significantly higher in forest topsoil compared to agricultural topsoil, whereas other properties were similar between forest and agriculture soils (Fig. 2ab). The intermediate SOC pool was the largest fraction in both topsoil and subsoil, accounting for 78 ± 13 % and 57 ± 17 % of total SOC, respectively, with sizes ranging from 3.3 to 27.0 g C kg^{-1} in topsoil and 0.5 to 3.7 g C kg^{-1} in subsoil. In contrast, the labile pool was the smallest, ranging from 0.1 to 1.2 g C kg^{-1} in topsoil and 0.01 to 0.09 g C kg^{-1} in subsoil. MRTs of intermediate SOC pools were decades to tens of decades with no significant difference between topsoil and subsoil (Table 3). Subsoil had significantly shorter MRTs ($P < 0.01$) for the labile pool (6 to 52 days) than topsoil (22 to 94 days). In terms of size and proportion, topsoil had higher levels of labile and intermediate SOC pools than subsoil (Fig. 2cd). By comparison, all pool sizes in both topsoil and subsoil were significantly lower in IGP than for tropical volcanic regions (VR, Fig. 2cd) we previously examined (Lyu et al., 2021b), especially the stable pool, which is linked to high active Al/Fe content in VR.

Fig. S8 shows correlation matrices to elucidate relationships between SOM fractions and SOC pools. The strongest correlation emerged between MAOM and C_I for both topsoil and subsoil ($r_s = 0.80^{**}$ and 0.87^{***}). In subsoil, MAOM was positively correlated with MRT_I (Fig. S8).

3.3. Contributions of land use, climatic and soil properties to SOM fractions and SOC pools

The potential determinants of SOM fractions and SOC pools for IGP soils are shown in Fig. 3. Land use demonstrated a strong positive correlation ($P < 0.01$) with LF in topsoil. Also, soil pH was negatively correlated with LF and oPOM ($r_s = -0.63^{*}$ and -0.66^{*}) in topsoil. As a conventional indicator of SOM quality, the C:N ratio was positively correlated with both the content and proportion of MAOM ($r_s = 0.59^{*}$ and 0.84^{***}). Positive correlations of clay, active Fe, and exchangeable Ca^{2+}/Mg^{2+}, were observed with MAOM in subsoil, with patterns similar to C_I.

MRT_I, which is indicative of the intermediate SOC pool stability, was higher in lower IGP and positively correlated with active Al/Fe, clay + silt, and clay ($r_s = 0.87^{***}$, 0.78^{**}, and 0.81^{**}; Fig. 3a) in topsoil. Similar to topsoil, MRT_I increased with the increase of active Al/Fe in subsoil ($r_s = 0.62^{*}$), whereas pH negatively contributed to MRT_I (Fig. 3b). In subsoil, clay and exchangeable Ca^{2+}/Mg^{2+} showed positive correlations with C_I ($r_s = 0.73^{**}$ and 0.59^{*}). Moreover, active Al/Fe showed a strong positive correlation with C_S ($r_s = 0.84^{***}$), as well as correlations with clay + silt and EP ($r_s = 0.78^{**}$ and 0.76^{**}) in subsoil, where pH was negatively correlated with C_S (Fig. 3b).

PLS-PM was applied to quantify the influence of climate, soil properties, and land use while accounting for confounding effects on the size and residence time of SOC pools (Fig. S9). Due to the significantly lower

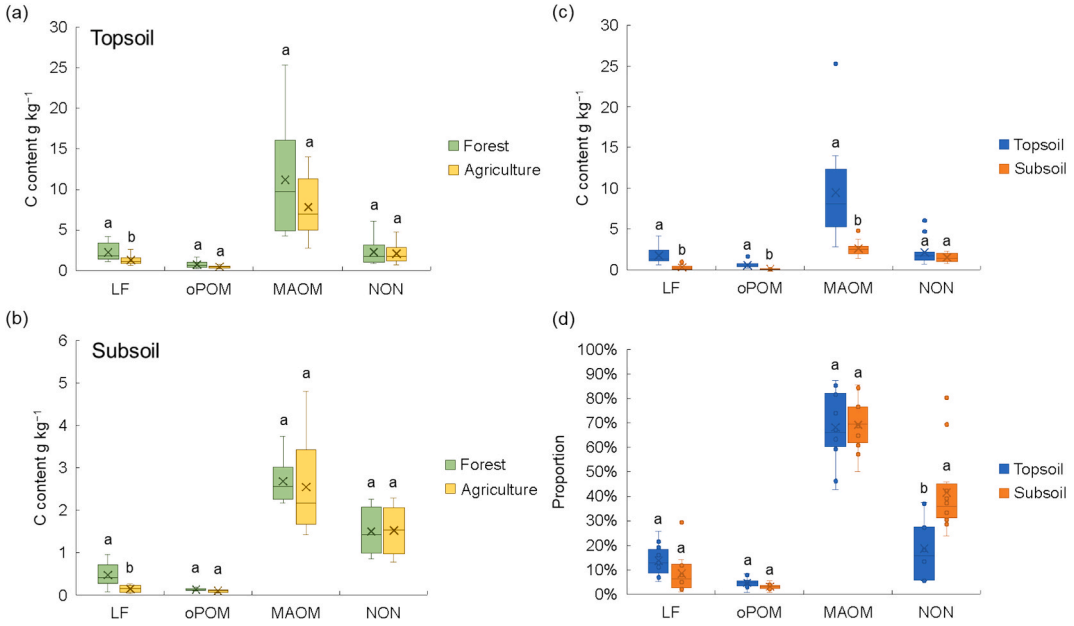

Fig. 1. Box diagrams of sizes for SOM fractions of forest and agriculture sites in topsoil (a) and subsoil (b), and sizes (c) and proportions (d) for SOM fractions in topsoil and subsoil across all sites. Lower-case letters indicate significant differences between forest and agriculture soils and between topsoil and subsoil ($P < 0.05$). × indicates the mean value. LF, light fraction; oPOM, occluded particulate organic matter in aggregates; MAOM, mineral-associated organic matter; NON, non-hydrolyzable MAOM, which is a subfraction of MAOM.

Table 3
Size, proportion and mean residence time of SOC pools for topsoil and subsoil horizons.

Topsoil		I1FT	I2FT	I3FT	I4FT	I5FT	I6FT	I1AT	I2AT	I3AT	I4AT	I5AT	I6AT
C_L	g kg^{-1}	0.42	1.21	0.28	0.31	0.19	0.25	0.69	0.09	0.31	0.28	0.19	0.57
C_I	g kg^{-1}	9.93	8.60	4.55	27.02	14.81	17.99	7.21	3.31	5.33	13.94	10.21	8.16
C_S	g kg^{-1}	6.08	2.17	1.83	1.58	0.85	1.09	4.73	1.29	2.11	2.21	0.66	1.35
C_L%		2.5	10.1	4.3	1.1	1.2	1.3	5.5	1.9	4.0	1.7	1.8	5.6
C_I%		60.5	71.8	68.3	93.5	93.5	93.1	57.1	70.6	68.8	84.9	92.2	80.9
C_S%		37.0	18.1	27.4	5.5	5.4	5.6	37.4	27.5	27.2	13.4	6.0	13.4
MRT_L	days	31	94	39	33	42	66	56	23	40	26	22	53
MRT_I	years	32.1	31.0	81.9	126.8	206.0	242.7	27.4	67.4	149.6	86.8	122.7	126.3
Subsoil		**I1FS**	**I2FS**	**I3FS**	**I4FS**	**I5FS**	**I6FS**	**I1AS**	**I2AS**	**I3AS**	**I4AS**	**I5AS**	**I6AS**
C_L	g kg^{-1}	0.04	0.05	0.02	0.07	0.02	0.07	0.04	0.01	0.04	0.08	0.09	0.01
C_I	g kg^{-1}	1.99	2.68	2.07	2.28	0.97	2.29	2.22	1.90	3.67	1.96	0.47	3.46
C_S	g kg^{-1}	1.31	0.85	1.53	1.02	2.26	2.02	1.33	0.77	1.98	1.04	2.28	1.74
C_L%		1.2	1.3	0.4	2.1	0.6	1.6	1.0	0.3	0.7	2.6	3.3	0.1
C_I%		59.6	74.9	57.3	67.6	29.9	52.3	61.8	71.2	64.5	63.6	16.4	66.5
C_S%		39.2	23.8	42.3	30.3	69.5	46.1	37.2	28.8	34.7	33.9	80.3	33.5
MRT_L	days	17	44	20	20	52	15	12	13	6	17	10	9
MRT_I	years	66.3	86.0	126.6	34.2	96.2	58.4	57.0	83.6	158.4	26.8	33.7	130.4

C_L, C_I, and C_S, size of labile, intermediate, and stable SOC pools, respectively; C_L%, C_I%, and C_S%, proportion of labile, intermediate, and stable SOC pools, respectively; MRT_L and MRT_I, mean residence time of labile and intermediate SOC pools.
I1 to I6, sampling location from the upper to lower IGP; FT, FS, AT, and AS refer to forest topsoil, forest subsoil, agricultural topsoil, and agricultural subsoil, respectively.

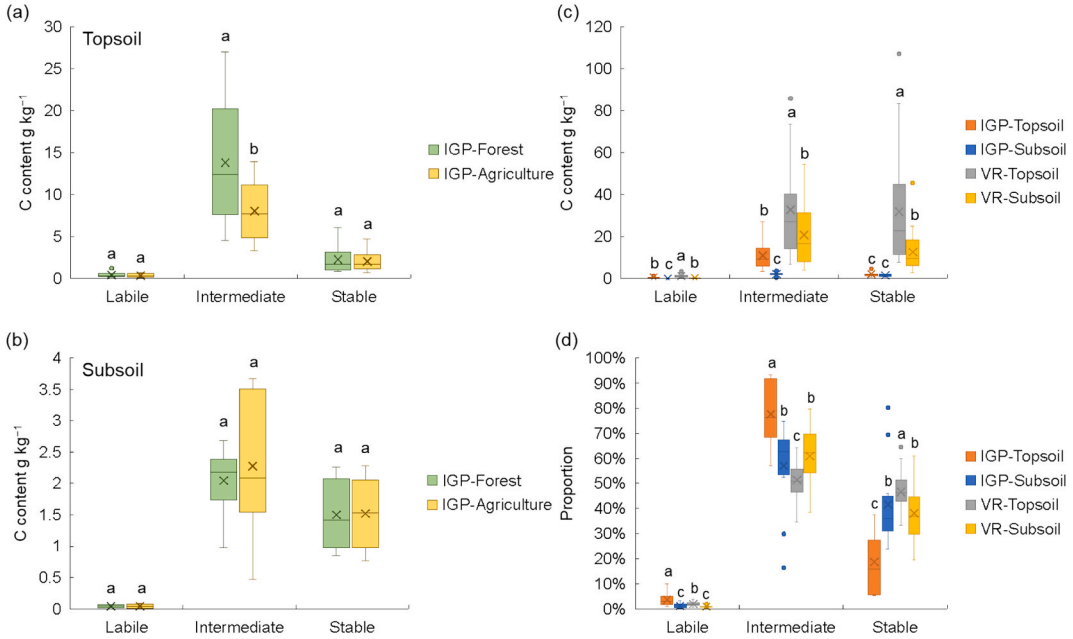

Fig. 2. Box diagrams of sizes for SOC pools of forest and agriculture sites in topsoil (a) and subsoil (b), and sizes (c) and proportions (d) for SOC pools in topsoil and subsoil from Indo-Gangetic plain (IGP, high pH and low active Al/Fe) and tropical volcanic regions (VR, low pH and high active Al/Fe). Lower-case letters indicate significant differences between forest and agriculture soils and differences for each pool among the soils ($P < 0.05$). × indicates the mean value. Data for VR soils are from our previous study (Lyu et al., 2021b).

C_I in agricultural topsoil, the impact of land use on C_I was also included in PLS-PM. The final PLS-PM analysis presents only the significant factors, as illustrated in Fig. 4. Mean residence time of the intermediate SOC pool (i.e., MRT_I) was well explained ($r^2 = 0.86$ and 0.48 for topsoil and subsoil), primarily by the direct contribution from active Al/Fe in both topsoil and subsoil ($\beta = 0.93$*** and 0.69**). Exchangeable Ca^{2+}/Mg^{2+} had no significant contribution to the size and mean residence time of any SOC pool (Figs. 4 and S9).

Land use (0 for agriculture, 1 for forest) positively contributed to C_I in topsoil and MRT_L in subsoil (Fig. 4). The C_I in subsoil had contributions exclusively from clay content ($\beta = 0.79$***, $r^2 = 0.63$), which was inversely related to elevation (i.e., river flow velocity/deposition; Fig. 4b). C_S in subsoil was well explained ($r^2 = 0.92$) and primarily contributed by active Al/Fe ($\beta = 0.63$***), which was negatively affected by soil pH (Fig. 4b). EP also manifested a positive contribution to C_S in subsoil ($\beta = 0.51$**) partially owing to its positive relationship with active Al/Fe.

3.4. SOM molecular composition evaluated by Py-GC/MS

SOM molecular composition was similar between agricultural and forest soils in topsoil or subsoil (Fig. S10). Consequently, we combined these datasets to probe the determinants of SOM composition. Delving into the specifics, forest soils revealed a higher proportion of degraded PS and long alkane (Table S3). The N-containing group was the predominant SOM component, followed by MAH and degraded PS (Fig. S11

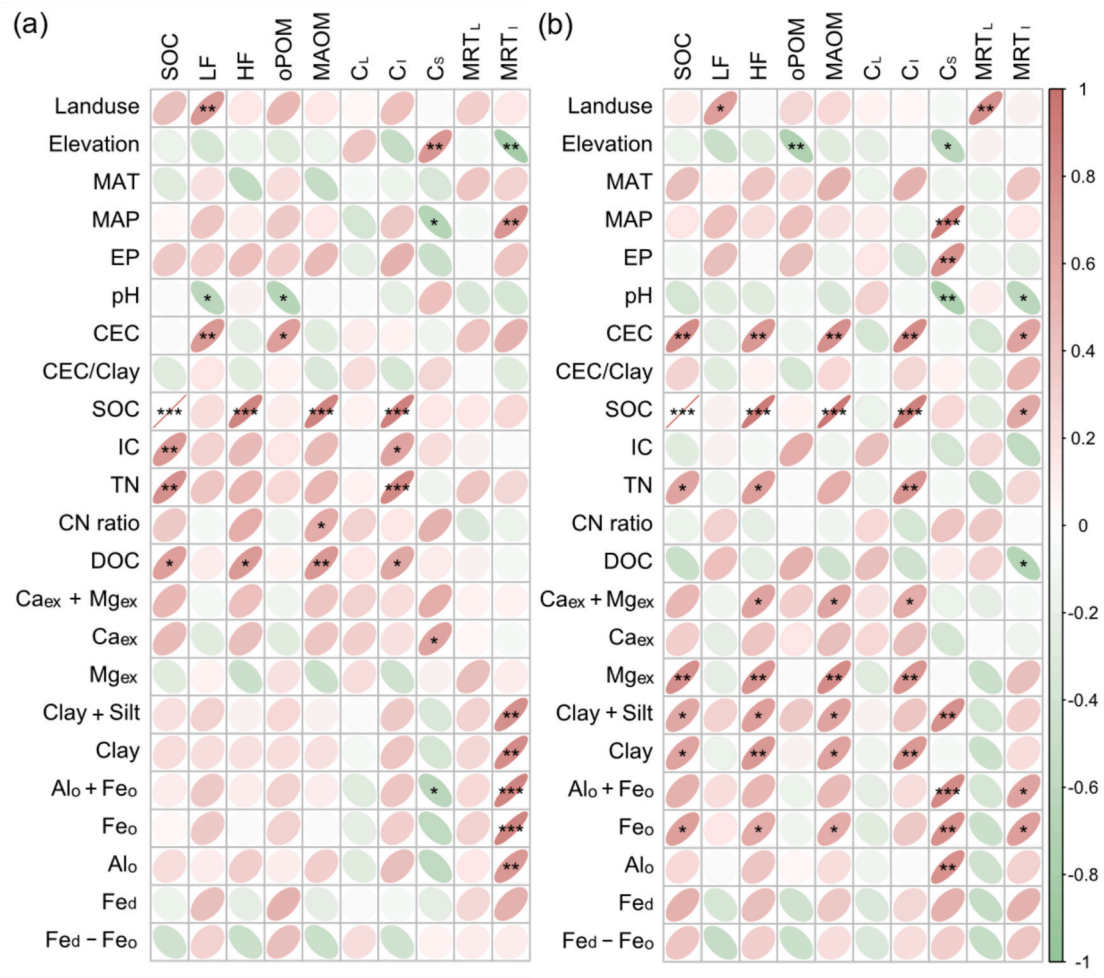

Fig. 3. Spearman correlation matrices (r_s) between organic carbon properties with climatic and geochemical properties for topsoil (a, $n = 12$) and subsoil (b, $n = 12$). Landuse, forest (1) and agriculture (0); MAT, mean annual temperature; MAP, mean annual precipitation; EP, excess precipitation; CEC, cation exchange capacity; SOC, soil organic carbon; IC, inorganic carbon; TN, total nitrogen; CN ratio, ratio of SOC to TN; DOC, dissolved organic carbon; $Ca_{ex} + Mg_{ex}$, exchangeable Ca^{2+} and Mg^{2+}; Fe_o and Al_o, acid oxalate extractable active Fe and Al; Fe_d, dithionite-citrate extractable iron; $Fe_d - Fe_o$, crystalline Fe (hydr)oxides. LF and HF, light and heavy fractions; oPOM, occluded particulate organic matter in aggregates; MAOM, mineral-associated organic matter. C_L, C_I, and C_S, size of labile, intermediate, and stable SOC pools, respectively; MRT_L and MRT_I, mean residence times of labile and intermediate SOC pools. The quantification of LF, HF, oPOM, and MAOM is based on carbon content.

and Table 4). Among aromatic hydrocarbons, the MAH proportion was larger than PAH in both topsoil (MAH: 12.5 ± 2.6 %, PAH: 1.5 ± 0.7 %) and subsoil (MAH: 16.9 ± 3.8 %, PAH: 0.8 ± 1.1 %). N-containing compounds were primarily composed of non-aromatic nitriles (44.4 ± 19.4 %) for all samples. Compounds in the degraded PS group were mainly heterocyclic compounds, such as furans (5.5 ± 2.5 % for all samples). Remarkably, no undegraded PS, a biomarker for cellulose and starch, was detected (Table 4). Lignin proportions were minimal in topsoil (1.2 ± 0.6 %) and were not detected in subsoil.

PERMANOVA results indicated a significant difference in SOM composition between topsoil and subsoil (Fig. S12). As illustrated in Table 4, subsoil demonstrated significantly lower degraded PS, lignin, and phenols but higher MAH than topsoil. Notably, lignin and phenol groups were absent in subsoil.

The RDA diagram (Fig. 5a) elucidated that climate, horizon, and soil physicochemical and mineralogical properties explained 74.6 % of SOM composition variation ($F = 2.89$, $P < 0.001$). The dominant RDA1 axis, encapsulating 58.1 % of the variance, was primarily shaped by SOC and differences between topsoil and subsoil, accompanied by a minor influence of moisture-associated factors like EP, pH, and active Al/Fe. Meanwhile, RDA2 (16.5 %) drew significant contributions from EP ($P < 0.001$), pH ($P < 0.01$), and active Al/Fe ($P < 0.05$). However, land use, clay, clay + silt, and exchangeable Ca^{2+}/Mg^{2+} did not significantly impact SOM composition ($P > 0.05$; Fig. 5a).

Topsoil exhibited lower RDA1 scores, indicating a higher abundance of degraded PS, lignin, and phenols but lower levels of MAH and N-containing groups (Fig. 5). The SOC content effectively distinguished topsoil from subsoil along the RDA1 axis. Factors like EP, pH, and active Al/Fe accentuated disparities in FAnE, n-alkanes, PAH, and N-containing compounds. Consistent with RDA, FAnE was positively correlated with EP and active Al/Fe in topsoil, but negatively correlated with pH (Fig. S13a). FAnE was also closely related to active Al and EP in subsoil ($r_s = 0.58$, $P = 0.05$; $r_s = 0.53$, $P = 0.07$). Long alkanes, representing less decomposed lipids, were positively correlated with EP in topsoil (Fig. S13a) and EP and active Al/Fe in subsoil (Fig. S13b).

4. Discussion

4.1. Characteristics of SOM fractions and SOC pools in IGP soils

SOC content in IGP soils was low, but direct controlling factors remain unclear (Fig. S2; Lal, 2004). Given the similarity in soil properties between forest and agricultural soils, data from both land-use types have been combined for discussion. Subsoil SOC content appears to be

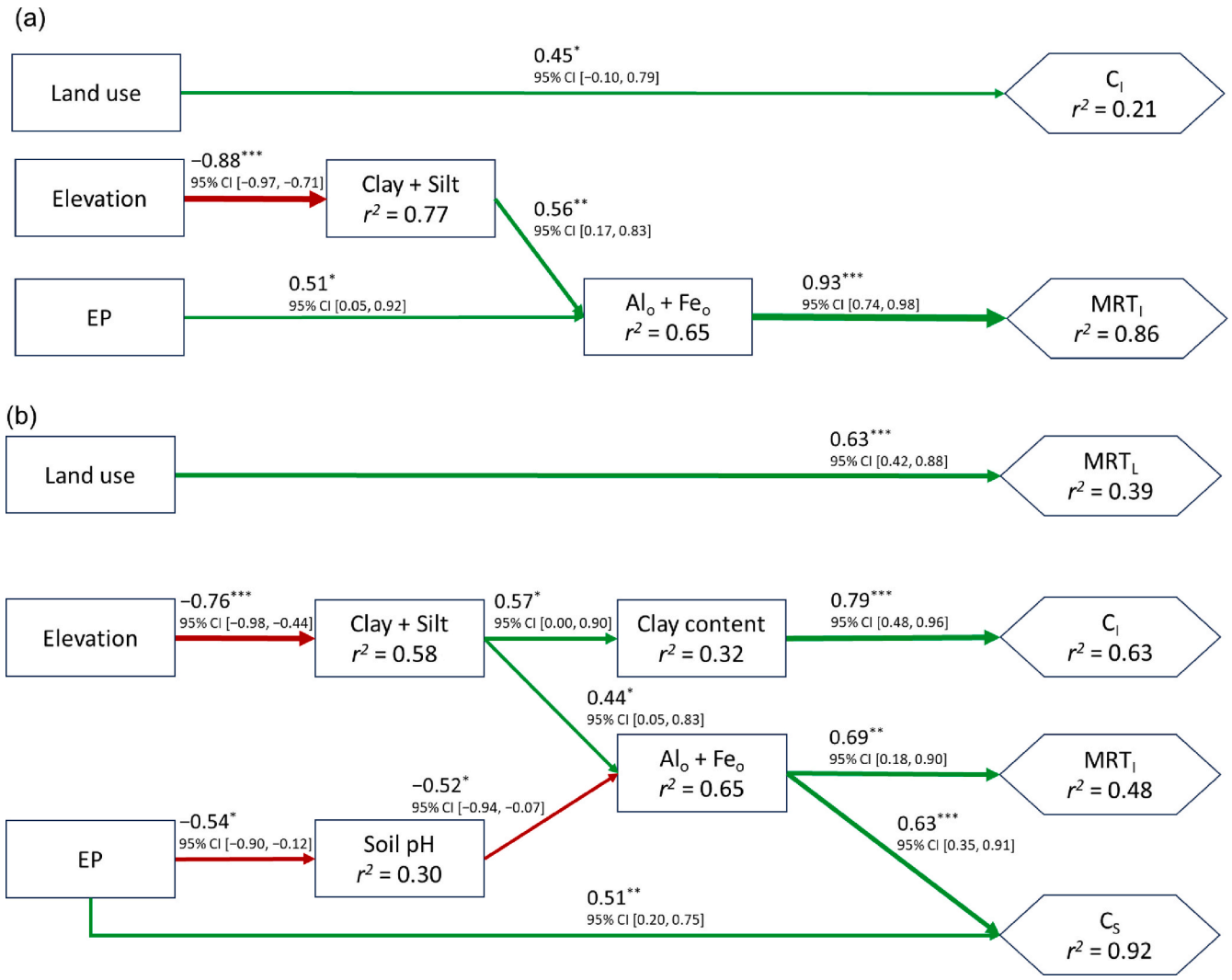

Fig. 4. Partial-least-squares path modeling revealing the contribution of climatic and geochemical properties on size and mean residence time (MRT) of SOC pools in topsoil (a, $n = 12$) and subsoil (b, $n = 12$). EP, excess precipitation; $Al_o + Fe_o$, oxalate-extractable active Al and Fe; MRT_L and MRT_I, mean residence times for labile and intermediate SOC pool representing their stabilities; C_I and C_S, size of intermediate and stable SOC pools. Only significant relationships were represented ($P < 0.05$); green and red colors represent positive and negative contributions, respectively; the number above the line and the line thickness represents the normalized path coefficient (β). A bootstrapping method provided the significance and the confidence interval (CI) of the path coefficient. (For interpretation of the references to colour in this figure legend, the reader is referred to the web version of this article.)

influenced by active Al/Fe, clay, and exchangeable Ca^{2+}/Mg^{2+} (Fig. S4b). However, in IGP topsoil, no conspicuous influence of climatic or soil properties on total SOC was observed (Fig. S4a). To decipher the underlying cause of low SOC in IGP soils, particularly within topsoil, a deeper exploration into the nuances of SOM was applied, including SOC pools, SOM fractions by fractionation, and molecular composition.

The intermediate SOC pool emerges as the predominant pool of total SOC (78 ± 13 % in topsoil and 57 ± 17 % in subsoil), thereby controlling overall SOC decomposition/storage over durations spanning years to decades (Table 3). The stable SOC pool is highly resistant to decomposition, contributing only 1.0 ± 1.1 % to cumulative CO_2 release during incubation (calculated using Eq. (S1)). Thus, intermediate SOC pool governs the mid-to-long-term SOC turnover. Similar dominance of this pool has been reported in temperate and tropical mineral soils where it controls decadal-scale turnover (Lyu et al., 2021b; Tian et al., 2016; Wang et al., 2017).

The larger size and proportion of intermediate SOC pool in topsoil compared to subsoil (Fig. 2) suggest that topsoil SOC storage depends more on this pool. The labile SOC pool, which influences short-term SOC dynamics (i.e., MRT_L, Table 3), generally reflects characteristics of organic matter input from vegetation (Lyu et al., 2021a; Wang et al., 2020). The marked contrast in MRT_L between the topsoil (44 ± 21 days) and subsoil (20 ± 14 days) indicates diminished labile pool stability in subsoil, potentially driven by an influx of more bioavailable DOC leaching from topsoil and root exudates (Angst et al., 2018; Sokol and Bradford, 2019).

Mineral associations are essential in neutral-to-alkaline soils to improve soil carbon accumulation and stability, both at our sites and in other studies (Rasmussen et al., 2018). At our sites, MAOM dominates total C in both horizons (Fig. 1d) and correlates positively with the C_I, confirming its central role in SOC storage and stability (Jamoteau et al., 2025; Rodrigues et al., 2022). Higher MAOM coincides with less labile C and a larger intermediate pool in topsoil, and with longer residence time of intermediate SOC pool in subsoil (Fig. S8), indicating the stabilizing role of mineral associations. A higher proportion of non-hydrolyzable MAOM (i.e., the stable SOC pool) in subsoil (Fig. 1d) further underscores a higher long-term stability/protection of subsoil SOC.

Table 4
Comparison of the relative abundance (mean ± SD, $n = 12$) of SOM compounds between topsoil and subsoil, as determined by pyrolysis–gas chromatography–mass spectrometry.

Orgnaic compounds	Topsoil (%)	Subsoil (%)	P value of paired *t*-test
Undegraded PS	n.d.	n.d.	–
Degraded PS	20.5 ± 8.5	6.3 ± 5.5	0.045
Long alkanes	0.7 ± 0.3	2.0 ± 0.9	0.009
Short alkanes	2.4 ± 0.8	1.7 ± 0.8	0.008
n-alkenes	3.3 ± 1.7	3.1 ± 2.4	0.024
Squalene	1.3 ± 1.0	6.9 ± 5.4	0.054
FAnE	0.7 ± 0.8	3.7 ± 6.3	0.063
Steroids	n.d.	0.2 ± 0.3	0.003
Lignin	1.2 ± 0.6	n.d.	<0.001
Phenols	4.5 ± 2.2	n.d.	<0.001
MAH	12.5 ± 2.6	16.9 ± 3.8	0.038
PAH	1.5 ± 0.7	0.8 ± 1.1	0.011
N-MAH	1.8 ± 0.5	1.1 ± 0.6	0.006
Alkylamides	1.0 ± 2.2	0.5 ± 1.6	0.016
N-containing	46.2 ± 12.4	56.4 ± 14.6	0.146
Other hydrocarbons	2.5 ± 1.9	0.3 ± 0.6	0.006

n.d., not detected; PS, polysaccharides; FAnE, fatty acids and their esters; MAH, monocyclic aromatic hydrocarbons; PAH, polycyclic aromatic hydrocarbons; N-MAH, N-containing MAH; N-containing, other N containing compounds.

4.2. Factors controlling SOC pools

Despite the minimal levels of active Al/Fe in neutral-to-alkaline soils compared to acidic soils, active Al/Fe appears essential for SOC content in IGP soils, consistent with our first hypothesis. Soils from the lower IGP had more active Al/Fe, corresponding to higher EP and clay and silt content (Figs. S2 and S4). Increased moisture (MAP and EP) lowers pH, thereby promoting active Al/Fe formation (Fig. 4; Lyu et al., 2022). Active Al/Fe contributes to SOC preservation in subsoil, as indicated by the positive relationship between active Al/Fe and SOC (Fig. S4b). Meanwhile, the significantly smaller intermediate and stable SOC pools in IGP soils (Fig. 2c) compared to tropical volcanic soils are likely due to its much lower active Al/Fe content (Table S2), which regulates these pools in tropical volcanic regions (Lyu et al., 2021b).

With regard to our first hypothesis, the active Al/Fe fraction positively regulates SOM stability, as revealed by the predominant contributions of active Al/Fe to MRT_I in both topsoil and subsoil (Fig. 4). Also, a significantly lower proportion of the stable pool in IGP topsoil compared to active Al/Fe-enriched volcanic topsoils (Fig. 2c) indicates lower SOC stability. The active Al/Fe fraction can preserve organic matter and increases the mean residence time of SOC through the formation of covalent bonds with organic matter on mineral surfaces (e.g., Fe (hydr)oxides), organic-metal complexes, and micro-aggregates (Churchman et al., 2020; Kleber et al., 2021).

The stabilizing effect of active Al/Fe on SOM was particularly pronounced in subsoil (Fig. 4), consistent with our second hypothesis. This may be due to the lower carbon-saturation status of subsoil minerals that increases their propensity for formation of inner-sphere complexes with SOM (McNally et al., 2018). The higher reactivity of subsoil minerals was supported by the enlarged stable SOC pool in subsoils with less-saturated active Al/Fe (i.e., lower SOC/(Al_o + Fe_o) ratio), in contrast to topsoil horizons. Interestingly, this study found that the SOC/(Al_o + Fe_o) ratio of 7.3 ± 3.3 in the neutral-to-alkaline subsoils (pH: 8.0 ± 1.1) was comparable to that observed in the acidic subsoils (SOC/(Al_o + Fe_o): 7.7 ± 4.7; pH: 5.1 ± 0.8) reported by Ashida et al. (2021). This similarity suggests that the capability of active Al/Fe to stabilize organic carbon in subsoil is consistently effective across acidic to alkaline soil pH levels.

Exchangeable Ca^{2+}/Mg^{2+} may enhance the stability of SOC, especially in alkaline soils (Carmeis Filho et al., 2017). However, probably due to the presence of shell-carbonate fragments in I4 and secondary $CaCO_3$ that affect exchangeable Ca^{2+} concentrations (Table S2), only exchangeable Mg^{2+} exhibited a positive correlation with SOC in subsoil (Fig. 3b). Exchangeable Ca^{2+} and Mg^{2+} can act as an ionic bridge, linking mineral surfaces with negative charges (i.e., clays) and SOM, thereby enhancing SOM stability. (Kleber et al., 2021). Though SOM interactions with clay minerals and exchangeable Ca^{2+}/Mg^{2+} may enlarge the intermediate SOC pool in subsoil (Fig. 3b), the influence of the former was more conspicuous (Fig. 4b). In subsoil, given the reduced SOC-to-clay ratio (i.e., SOC saturation), more SOM appears to be stabilized directly on clay surfaces, thereby contributing to a larger intermediate SOC pool (Fig. 4b).

Ca and Mg ions link charged clay and organic matter, but their effect is weaker than active Al/Fe for SOM preservation, as indicated by a strong correlation between C_S and active Al/Fe, versus no significant

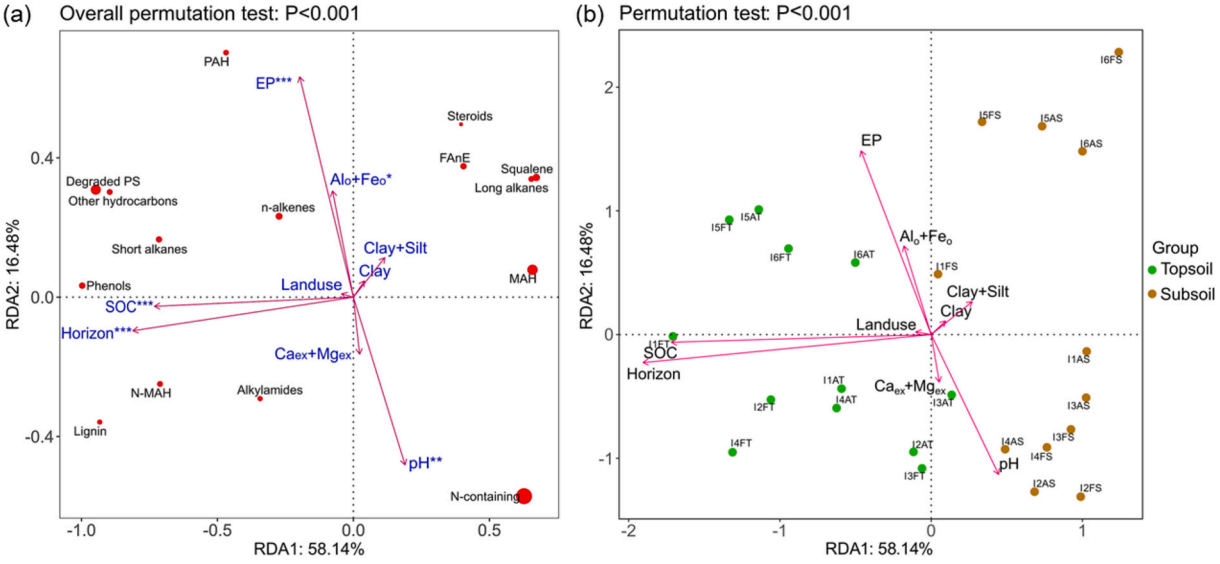

Fig. 5. Redundancy analysis (RDA) diagram showing SOM compound groups and their controls (a), and the diagram showing the distribution of SOM composition across all soils (b). EP, excess precipitation; Horizon, topsoil (1) and subsoil (0); Landuse, forest (1) and agriculture (0); Ca_{ex} + Mg_{ex}, exchangeable Ca^{2+} and Mg^{2+}; Al_o + Fe_o, oxalate-extractable active Al and Fe; PS, polysaccharides; FAnE, fatty acids and esters; MAH, monocyclic aromatic hydrocarbons; PAH, polycyclic aromatic hydrocarbons, N-MAH, N-containing MAH; N-containing, other N-containing compounds; FT, FS, AT, and AS refer to forest topsoil, forest subsoil, agricultural topsoil, and agricultural subsoil, respectively. I1 to I6, sampling location from the upper to lower IGP.

correlation with Ca^{2+}/Mg^{2+} (Fig. 3b and 4b). The significant contribution of active Al/Fe, as opposed to exchangeable Ca^{2+}/Mg^{2+}, to the stability of intermediate SOC pool (i.e., MRT_I) also indicates the stronger ability of active Al/Fe in stabilizing OM (Fig. 4). Additionally, the strong positive contribution of EP to the size of the stable pool in subsoil may result from greater mineral-associated OM translocation together with clay translocation from topsoil to subsoil in soils with higher EP (Fig. 4b).

Neutral-to-alkaline pH values enhance enzyme activities (Puissant et al., 2019) involved in litter decomposition and also limit the formation of active Al/Fe that stabilizes OM (Candra et al., 2019). Higher soil pH resulted in reduced stability of the intermediate SOC pool (i.e., MRT_I) in subsoil horizons (Fig. 3b), and less LF and oPOM remained in topsoil horizons (Fig. 3a).

In the agricultural topsoil of the IGP, reduced litter inputs and increased physical disturbance led to a reduced intermediate SOC pool (Fig. 2a and 4a), contributing to significant SOC loss, which supports our third hypothesis. Tillage is considered sufficient to break macro-aggregates, expose the mineral-associated OM that dominates the intermediate pool (Fig. S8a), and accelerate its depletion. By contrast, the free labile fraction is already minimal regardless of cultivation history (Table 3), and the non–hydrolyzable MAOC (the stable SOC pool), which should be controlled by active Al/Fe (Fig. 4), is strongly sorbed to the mineral inner surface and chemically stable (Paul et al., 2001), leaving both pools largely unaffected by agricultural activity. This effect, however, was not significant in subsoil (Fig. 2b), where soils are less disturbed and minerals play an essential role. Partially refuting our third hypothesis, agricultural activity reduced LF in both topsoil and subsoil and decreased the stability of the labile SOC pool in subsoil, which depends highly on input. Therefore, the application of active Al/Fe-bearing soil amendments, along with strategies to enhance deep organic matter inputs—such as introducing deep-rooting perennial crops and placing compost in the subsoil—could be considered as potential approaches, although they warrant further investigation and investment (Peixoto et al., 2022).

4.3. Insights from SOM molecular composition

SOM in both agricultural and forest sites in IGP were highly degraded, as evidenced by a predominant proportion of N-containing compounds, followed by MAH, and limited detection of less degraded compounds like undegraded PS (Fig. S11 and Table S3) (Buurman and Roscoe, 2011; Lu et al., 2018). The significantly higher proportion of the N-containing group in neutral-to-alkaline IGP soils compared to soils with lower pH (Girona-García et al., 2019; Lyu et al., 2024) suggests a high degree of SOM degradation, which can be attributed to elevated pH that limits the formation of active Al/Fe and enhances microbial activity, reducing SOM stabilization.

The absence of undegraded PS (e.g., cellulose) further supports the intensive microbial degradation of SOM in neutral-to-alkaline IGP soils. Although lignin is typically resistant to decomposition (Marschner et al., 2008), its intensive degradation in tropical soils with high temperatures (Vancampenhout et al., 2009), aligns with its limited abundance in IGP soils (Fig. S11 and Table 4). However, the drier conditions in IGP may attenuate lignin degradation somewhat, as suggested by a slightly higher lignin proportion in IGP (1.2 ± 0.6 %) than in more humid tropical topsoil (0.7 ± 0.7 %) (Lyu et al., 2024). Additionally, the significantly lower PAH level compared to MAH (Table 4) suggests limited aromatic polymerization, similar to findings in tropical regions (Lyu et al., 2024), challenging conventional humification concepts (Lehmann and Kleber, 2015).

Active Al/Fe emerged as a key factor influencing SOM composition, while clay and exchangeable Ca^{2+}/Mg^{2+} played lesser roles. The impact of active Al/Fe can be observed via its stabilization of less-degraded and less-recalcitrant OM, such as FAnE and long alkanes, and reduced levels of N-containing compounds (Figs. 5 and S13). This stabilization results from organo-mineral interactions and physical protection through aggregation, both strongly regulated by active Al/Fe (Rasmussen et al., 2018; Wagai et al., 2020). The biochemical stability of fatty acids, which are easily decomposed, may be further strengthened via hydrogen bonding with active Al/Fe (Figs. 5a and S13) (Kleber et al., 2021). Higher moisture and base-cation leaching reduce soil pH, promoting active Al/Fe formation, which stabilizes less-recalcitrant OM, likely within the intermediate SOC pool.

Under the condition of low active Al/Fe content, as seen in upper IGP regions with higher pH, more degraded compounds were prevalent (Fig. 5a), thereby supporting our first hypothesis. The near-neutral pH (Table S2) enhances microbial enzyme activity, such as acetylesterase, leading to increased SOM degradation (Puissant et al., 2019) and accumulation of N-containing compounds as residues (Fig. 5a). The importance of clay and clay + silt contents in stabilizing weakly degraded OM appears minimal (not significant, Fig. 5a). Similarly, exchangeable Ca^{2+}/Mg^{2+} does not appear to substantially influence the overall SOM composition (Fig. 5a).

Subsoil SOM in IGP was more degraded than topsoil, as evaluated using pyrolysis-GC/MS (Figs. 5 and S11, Table 4). The SOM composition of subsoil had elevated levels of N-containing compounds and MAH and lower levels of less degraded compounds (Carr et al., 2013; Lyu et al., 2024). Furthermore, RDA1 indicated a lower proportion of less-degraded compounds in subsoil (Fig. 5, Table 4). These results support a higher degree of SOM degradation in subsoil, which is consistent with our second hypothesis.

Subsoil SOM is more degraded and contains a larger proportion of microbial derivatives (Fig. 5; Table 4), a trend also influenced by the limited input of fresh litter to the subsoil compared to topsoil. Also, high soil pH and active microbial processing in IGP can increase OM solubility and mobility, facilitating the downward transport of degraded organic matter from topsoil to subsoil (Curtin et al., 2016). Compared to low pH subsoils (Girona-García et al., 2019; Lyu et al., 2024), neutral-to-alkaline IGP subsoil lacked phenols, degradation products of lignin and tannin, and had significantly lower levels of degraded PS, further indicating the highly degraded nature of SOM (Table 4). The reduced lignin and phenol proportions in IGP subsoil may be attributed to the metabolic activities of microbes like Actinomycetes and lignin-degrading fungi, including Ascomycetes, which degrade recalcitrant compounds in low-carbon environments (Fierer et al., 2007). Further investigation is needed to clarify microbial contributions.

Although cultivation can accelerate SOM degradation (Mganga and Kuzyakov, 2018), its impact appears limited in IGP, partially refuting our third hypothesis. Degraded PS and long alkanes were lower in agricultural soils compared to forest soils (Table S3; $P < 0.01$ and 0.05, respectively), suggesting that agriculture limits organic matter inputs and may accelerate the degradation of plant materials. Nevertheless, land use had no significant effect on overall SOM composition, which was similar between agricultural and forest soils (Figs. 5a and S10).

5. Conclusion

Our results identify active Al/Fe as the pivotal control on long-term SOC stabilization in the neutral-to-alkaline IGP soils. The intermediate SOC pool, which has a high affinity for MAOM C and serves as the largest SOC pool, derives its multi-decadal stability chiefly from interactions with active Al/Fe, rather than other clay minerals or exchangeable Ca^{2+}/Mg^{2+}, in both topsoil and subsoil. In subsoils, the proportion of stable SOC rises, yet its absolute amount is still controlled by active Al/Fe availability, underscoring the indispensable role of these phases under low C-saturation conditions. Notably, the protective efficiency of Al/Fe persists across acidic to alkaline soils, whereas clay and Ca^{2+}/Mg^{2+} exert little influence on either SOC stability. Agricultural disturbance accelerates SOC loss in topsoil by depleting the intermediate pool, whereas subsoil carbon is comparatively resilient—protected by Al/Fe–organic complexes under low C saturation—highlighting subsoil as a

promising target for further SOC stabilization. Intensive SOM degradation in IGP soils is likely due to low active Al/Fe levels and enhanced microbial activity resulting from neutral-to-alkaline pH. In contrast, exchangeable Ca^{2+}/Mg^{2+}, clay content, and agricultural activity have minimal effects on SOM composition.

In conclusion, high pH and low active Al/Fe fraction lead to reduced mid- to long-term SOC stability and intensive SOM degradation, resulting in low SOC in neutral-to-alkaline IGP soils. Agricultural activity further exacerbates SOC loss in topsoil. Our combined use of SOC pool-size/stability quantification and pyrolysis-GC/MS links SOC stability to its controlling factors and molecular composition, yet the study is correlative and confined to a single region. Multi-region and experimental trials are needed to confirm and broaden these insights.

Declaration of Generative AI and AI-assisted technologies in the writing process

During the preparation of this work the author(s) used GPT-4 in order to improve language and readability. After using this tool/service, the author(s) reviewed and edited the content as needed and take(s) full responsibility for the content of the publication.

CRediT authorship contribution statement

Ruohan Zhong: Writing – review & editing, Writing – original draft, Visualization, Investigation, Funding acquisition, Formal analysis, Data curation. **Han Lyu:** Writing – review & editing, Visualization, Methodology, Funding acquisition, Formal analysis, Data curation, Conceptualization. **Monika Kumari:** Resources, Formal analysis. **Ajay Kumar Mishra:** Writing – review & editing, Resources. **M.L. Jat:** Writing – review & editing, Resources. **Randy A. Dahlgren:** Writing – review & editing, Supervision, Resources. **Shinya Funakawa:** Writing – review & editing, Supervision, Resources, Project administration, Funding acquisition. **Tetsuhiro Watanabe:** Writing – review & editing, Supervision, Resources, Project administration, Methodology, Funding acquisition, Conceptualization.

Declaration of competing interest

The authors declare that they have no known competing financial interests or personal relationships that could have appeared to influence the work reported in this paper.

Acknowledgments

This work was supported by JSPS KAKENHI Grant Numbers 17H06171, 19J14696, 20H04322, 23H03524, 24K23918 and JST SPRING Grant Number JPMJSP2110. We gratefully appreciate the collaborative efforts of Indian Council of Agricultural Research and International Maize and Wheat Improvement Center. Special thanks go to Dr. Ummed Singh (ICAR-Indian Institute of Pulses Research, Kanpur); Dr. R. K. Jat (Borlaug Institute of South Asia, Samastipur, Bihar); Dr. A. K. Sinha (Uttar Banga Krishi Vishwavidyalaya, Cooch Behar, West Bengal); and Dr. H. S. Jat, Dr. B. Maji, and Dr. T. D. Lama (ICAR-Central Soil Salinity Research Institute, Karnal and Canning Town). We also appreciate the invaluable insights and assistance from numerous other researchers and community members during soil sampling within the study area.

Appendix A. Supplementary data

Supplementary data to this article can be found online at https://doi.org/10.1016/j.catena.2025.109215.

Data availability

Original data can be found online at: https://doi.org/10.17632/pc3f8rxtr2.1

References

Angst, G., et al., 2018. Soil organic carbon stocks in topsoil and subsoil controlled by parent material, carbon input in the rhizosphere, and microbial-derived compounds. Soil Biol. Biochem. 122, 19–30. https://doi.org/10.1016/j.soilbio.2018.03.026.

Angst, G., Mueller, K.E., Nierop, K.G.J., Simpson, M.J., 2021. Plant- or microbial-derived? a review on the molecular composition of stabilized soil organic matter. Soil Biol. Biochem. 156, 108189. https://doi.org/10.1016/j.soilbio.2021.108189.

Ashida, K., et al., 2021. Quantitative relationship between organiccarbon and geochemical properties in tropical surface and subsurface soils. Biogeochemistry 155, 77–95. https://doi.org/10.1007/s10533-021-00813-8.

Buurman, P., Roscoe, R., 2011. Different chemical composition of free light, occluded light and extractable SOM fractions in soils of cerrado and tilled and untilled fields, Minas Gerais, Brazil: a pyrolysis-GC/MS study. Eur. J. Soil Sci. 62, 253–266. https://doi.org/10.1111/j.1365-2389.2010.01327.x.

Candra, I.N., et al., 2019. Weathering and soil formation in rhyolitic tephra along a moisture gradient on alcedo volcano, galápagos. Geoderma 343, 215–225. https://doi.org/10.1016/j.geoderma.2019.01.051.

Carmeis Filho, A.C., Penn, C.J., Crusciol, C.A., Calonego, J.C., 2017. Lime and phosphogypsum impacts on soil organic matter pools in a tropical Oxisol under long-term no-till conditions. Agric., Ecosyst. Environ. 241, 11–23. https://doi.org/10.1016/j.agee.2017.02.027.

Carr, A.S., et al., 2013. Biome-scale characterisation and differentiation of semi-arid and arid zone soil organic matter compositions using pyrolysis–GC/MS analysis. Geoderma 200–201, 189–201. https://doi.org/10.1016/j.geoderma.2013.02.012.

Churchman, G.J., Singh, M., Schapel, A., Sarkar, B., Bolan, N., 2020. Clay minerals as the key to the sequestration of carbon in soils. Clay Clay Miner. 68, 135–143. https://doi.org/10.1007/s42860-020-00071-z.

Curtin, D., Peterson, M.E., Anderson, C.R., 2016. pH-dependence of organic matter solubility: base type effects on dissolved organic C, N, P, and S in soils with contrasting mineralogy. Geoderma 271, 161–172. https://doi.org/10.1016/j.geoderma.2016.02.009.

Davidson, E.A., Janssens, I.A., 2006. Temperature sensitivity of soil carbon decomposition and feedbacks to climate change. Nature 440, 165–173. https://doi.org/10.1038/nature04514.

Doetterl, S., et al., 2015. Soil carbon storage controlled by interactions between geochemistry and climate. Nat. Geosci. 8, 780–783. https://doi.org/10.1038/Ngeo2516.

Dungait, J.A., Hopkins, D.W., Gregory, A.S., Whitmore, A.P., 2012. Soil organic matter turnover is governed by accessibility not recalcitrance. Glob. Chang. Biol. 18, 1781–1796. https://doi.org/10.1111/j.1365-2486.2012.02665.x.

Fick, S.E., Hijmans, R.J., 2017. WorldClim 2: new 1-km spatial resolution climate surfaces for global land areas. Int. J. Climatol. 37, 4302–4315. https://doi.org/10.1002/joc.5086.

Fierer, N., Bradford, M.A., Jackson, R.B., 2007. Toward an ecological classification of soil bacteria. Ecology 88, 1354–1364. https://doi.org/10.1890/05-1839.

Girona-García, A., Badía-Villas, D., Jiménez-Morillo, N.T., González-Pérez, J.A., 2019. Changes in soil organic matter composition after scots pine afforestation in a native european beech forest revealed by analytical pyrolysis (py-GC/MS). Sci. Total Environ. 691, 1155–1161. https://doi.org/10.1016/j.scitotenv.2019.07.229.

Hair, J.F., et al., 2021. The SEMinR package. In: Hair Jr, J.F. (Ed.), Partial Least Squares Structural Equation Modeling (PLS-SEM) Using r: A Workbook. Springer International Publishing, Cham, pp. 49–74.

Harkin, D.A., 1960. The rungwe volcanics at the northern end of Lake Nyasa. Government Printer Dar es Salaam, Dar Es Salaam.

IUSS Working Group WRB, 2022. World Reference Base for soil resources, international soil classification system for naming soils and creating legends for soil maps. International Union of Soil Sciences (IUSS), Vienna, Austria.

Jamoteau, F., Kansiz, M., Unger, M., Keiluweit, M., 2025. Probing mineral-organic Interfaces in soils and sediments using optical photothermal infrared microscopy. Environ. Sci. Tech. 59, 501–512. https://doi.org/10.1021/acs.est.4c09258.

Jia, J., et al., 2023. Relationships between soil biodiversity and multifunctionality in croplands depend on salinity and organic matter. Geoderma 429, 116273. https://doi.org/10.1016/j.geoderma.2022.116273.

John, B., Yamashita, T., Ludwig, B., Flessa, H., 2005. Storage of organic carbon in aggregate and density fractions of silty soils under different types of land use. Geoderma 128, 63–79. https://doi.org/10.1016/j.geoderma.2004.12.013.

Keiluweit, M., et al., 2015. Mineral protection of soil carbon counteracted by root exudates. Nat. Clim. Chang. 5, 588–595. https://doi.org/10.1038/nclimate2580.

Kleber, M., et al., 2021. Dynamic interactions at the mineral–organic matter interface. Nat. Rev. Earth Environ. 2, 402–421. https://doi.org/10.1038/s43017-021-00162-y.

Lal, R., 2004. Soil carbon sequestration in India. Clim. Change 65, 277–296. https://doi.org/10.1023/B:Clim.0000038202.46720.37.

Lal, R., 2010. Managing soils and ecosystems for mitigating anthropogenic carbon emissions and advancing global food security. Bioscience 60, 708–721. https://doi.org/10.1525/bio.2010.60.9.8.

Lehmann, J., Kleber, M., 2015. The contentious nature of soil organic matter. Nature 528, 60–68. https://doi.org/10.1038/nature16069.

Liu, C., Cui, Y., Li, X., Yao, M., 2021. microeco: an R package for data mining in microbial community ecology. FEMS Microbiol. Ecol. 97, fiaa255. https://doi.org/10.1093/femsec/fiaa255.
Lozano-García, B., Muñoz-Rojas, M., Parras-Alcántara, L., 2017. Climate and land use changes effects on soil organic carbon stocks in a Mediterranean semi-natural area. Sci. Total Environ. 579, 1249–1259. https://doi.org/10.1016/j.scitotenv.2016.11.111.
Lu, X., Ma, S., Chen, Y., Yangzom, D., Jiang, H., 2018. Squalene found in Alpine grassland soils under a harsh environment in the tibetan Plateau, China. Biomolecules 8. https://doi.org/10.3390/biom8040154.
Lützow, M.V., et al., 2006. Stabilization of organic matter in temperate soils: mechanisms and their relevance under different soil conditions - a review. Eur. J. Soil Sci. 57, 426–445. https://doi.org/10.1111/j.1365-2389.2006.00809.x.
Lyu, H., Watanabe, T., Kilasara, M., Funakawa, S., 2018. Effects of climate on distribution of soil secondary minerals in volcanic regions of Tanzania. Catena 166, 209–219. https://doi.org/10.1016/j.catena.2018.04.005.
Lyu, H., Watanabe, T., Kilasara, M., Hartono, A., Funakawa, S., 2021a. Soil organic carbon pools controlled by climate and geochemistry in tropical volcanic regions. Sci. Total Environ. 761, 143277. https://doi.org/10.1016/j.scitotenv.2020.143277.
Lyu, H., et al., 2022. Climatic controls on soil clay mineral distributions in humid volcanic regions of Sumatra and Java, Indonesia. Geoderma 425, 116058. https://doi.org/10.1016/j.geoderma.2022.116058.
Lyu, H., et al., 2021b. Factors controlling sizes and stabilities of subsoil organic carbon pools in tropical volcanic soils. Sci. Total Environ. 769, 144842. https://doi.org/10.1016/j.scitotenv.2020.144842.
Lyu, H., et al., 2024. Impact of climate on soil organic matter composition in soils of tropical volcanic regions revealed by EGA-MS and py-GC/MS. Environ. Sci. Tech. 58, 9646–9657. https://doi.org/10.1021/acs.est.3c07000.
Marschner, B., et al., 2008. How relevant is recalcitrance for the stabilization of organic matter in soils? J. Plant Nutr. Soil Sci. 171, 91–110. https://doi.org/10.1002/jpln.200700049.
McNally, S., et al., 2018. Assessing the vulnerability of organic matter to C mineralisation in pasture and cropping soils of New Zealand. Soil Res. 56, 481–490. https://doi.org/10.1071/SR17148.
Mganga, K.Z., Kuzyakov, Y., 2018. Land use and fertilisation affect priming in tropical andosols. Eur. J. Soil Biol. 87, 9–16. https://doi.org/10.1016/j.ejsobi.2018.04.001.
Neina, D., 2019. The role of soil pH in plant nutrition and soil remediation. Appl. Environ. Soil Sci. 2019, 5794869. https://doi.org/10.1155/2019/5794869.
Oksanen, J. et al., 2020. vegan community ecology package version 2.5-7 November 2020.
Pal, D.K., Bhattacharyya, T., Srivastava, P., Chandran, P., Ray, S.K., 2009. Soils of the indo-Gangetic Plains: their historical perspective and management. Curr. Sci. 96, 1193–1202.
Paul, E., Morris, S., Bohm, S., 2001. The determination of soil C pool sizes and turnover rates: Biophysical fractionation and tracers, Assessment Methods for Soil Carbon, CRC Press, Boca Raton, pp. 193-206.
Peixoto, L., et al., 2022. Deep-rooted perennial crops differ in capacity to stabilize C inputs in deep soil layers. Sci. Rep. 12, 5952. https://doi.org/10.1038/s41598-022-09737-1.
Possinger, A.R., et al., 2021. Climate effects on subsoil carbon loss mediated by soil chemistry. Environ. Sci. Tech. 55, 16224–16235. https://doi.org/10.1021/acs.est.1c04909.
Puissant, J., et al., 2019. The pH optimum of soil exoenzymes adapt to long term changes in soil pH. Soil Biol. Biochem. 138, 107601. https://doi.org/10.1016/j.soilbio.2019.107601.
Rasmussen, C., et al., 2018. Beyond clay: towards an improved set of variables for predicting soil organic matter content. Biogeochemistry 137, 297–306. https://doi.org/10.1007/s10533-018-0424-3.
Rodrigues, L.A.T., et al., 2022. Carbon saturation deficit and litter quality drive the stabilization of litter-derived C in mineral-associated organic matter in long-term no-till soil. Catena 219, 106590. https://doi.org/10.1016/j.catena.2022.106590.
Schmidt, M.W., et al., 2011. Persistence of soil organic matter as an ecosystem property. Nature 478, 49–56. https://doi.org/10.1038/nature10386.
Shah, S.H., et al., 2019. Does household capital mediate the uptake of agricultural land, crop, and livestock adaptations? Evidence from the indo-Gangetic Plains (India). Front. Sustain. Food Syst. 3–2019. https://doi.org/10.3389/fsufs.2019.00001.
Singh, A., Vishnoi, A.S., Banday, A.H., Bora, P., Pandey, P., 2023. Influence of stubble burning on air quality of northern India: a case study of indo-gangetic plains of India. Environ Monit Assess 195, 487. https://doi.org/10.1007/s10661-023-11027-w.
Six, J., Jastrow, J., 2002. Organic matter turnover. In: Lal, R. (Ed.), Encyclopedia of Soil Science. CRC Press, Boca Raton, FL, pp. 936-942.
Sokol, N.W., Bradford, M.A., 2019. Microbial formation of stable soil carbon is more efficient from belowground than aboveground input. Nat. Geosci. 12, 46–53. https://doi.org/10.1038/s41561-018-0258-6.
Thornthwaite, C.W., 1948. An approach toward a rational classification of climate. Geogr. Rev. 38, 55–94. https://doi.org/10.2307/210739.
Tian, Q., et al., 2016. Factors controlling soil organic carbon stability along a temperate forest altitudinal gradient. Sci. Rep. 6, 18783. https://doi.org/10.1038/srep18783.
Tiessen, H., Cuevas, E., Chacon, P., 1994. The role of soil organic matter in sustaining soil fertility. Nature 371, 783–785. https://doi.org/10.1038/371783a0.
Trumbore, S., 2000. Age of soil organic matter and soil respiration: radiocarbon constraints on belowground C dynamics. Ecol. Appl. 10, 399–411. https://doi.org/10.1890/1051-0761(2000)010[0399:Aosoma]2.0.Co;2.
Vancampenhout, K., et al., 2009. Differences in chemical composition of soil organic matter in natural ecosystems from different climatic regions – a pyrolysis–GC/MS study. Soil Biol. Biochem. 41, 568–579. https://doi.org/10.1016/j.soilbio.2008.12.023.
Wagai, R., Kajiura, M., Asano, M., 2020. Iron and aluminum association with microbially processed organic matter via meso-density aggregate formation across soils: organo-metallic glue hypothesis. Soil 2020, 1–42. https://doi.org/10.5194/soil-2020-32.
Wang, X., et al., 2020. Distinct regulation of microbial processes in the immobilization of labile carbon in different soils. Soil Biol. Biochem. 142. https://doi.org/10.1016/j.soilbio.2020.107723.
Wang, X.Y., et al., 2017. Regional patterns and controls of soil organic carbon pools of croplands in China. Plant and Soil 421, 525–539. https://doi.org/10.1007/s11104-017-3462-z.
Wiedemeier, D.B., Bloesch, U., Hagedorn, F., 2012. Stable forest-savanna mosaic in north-western Tanzania: local-scale evidence from δ13C signatures and 14C ages of soil fractions. J. Biogeogr. 39, 247–257. https://doi.org/10.1111/j.1365-2699.2011.02583.x.
Wikramanayake, E.D., 2002. Terrestrial ecoregions of the indo-Pacific: a conservation assessment. Island Press.
Xu, T., et al., 2021. Grassland degradation with saline-alkaline reduces more soil inorganic carbon than soil organic carbon storage. Ecol. Ind. 131, 108194. https://doi.org/10.1016/j.ecolind.2021.108194.
Yu, G., et al., 2017. Mineral availability as a key regulator of soil carbon storage. Environ. Sci. Tech. 51, 4960–4969. https://doi.org/10.1021/acs.est.7b00305.
Zhang, S., Yu, Z., Lin, J., Zhu, B., 2020. Responses of soil carbon decomposition to drying-rewetting cycles: a meta-analysis. Geoderma 361, 114069. https://doi.org/10.1016/j.geoderma.2019.114069.
Zhong, R., et al., 2023. Contributions of fine mineral particles and active Al/Fe to stabilization of plant material in neutral-to-alkaline soils of indo-gangetic plain. Geoderma 440, 116709. https://doi.org/10.1016/j.geoderma.2023.116709.